



**Similarity of extremely rare nonequilibrium processes to equilibrium processes**Peter Werner and Alexander K. Hartmann *Institut für Physik, Universität Oldenburg, 26111 Oldenburg, Germany* (Received 24 November 2020; revised 30 August 2021; accepted 31 August 2021; published 10 September 2021)

For system coupled to heat baths, typical nonequilibrated processes, e.g., induced by varying an external parameter without waiting for equilibration in between, are very different from the corresponding equilibrium infinitely slow processes. Nevertheless, there are connections between equilibrium and nonequilibrated behaviors, e.g., the theorems of Jarzynski and Crooks, which relate the distribution  $P(W)$  of nonequilibrium work to the free energy differences  $\Delta F$ . Here we study the naturally arising question, whether those relevant but rare trajectories, which exhibit these work values, show a higher degree of similarity to equilibrium. For convenience, we have chosen a simple model of RNA secondary structures (or single-stranded DNA), here modeling a medium-size hairpin structure, under influence of a varying external force. This allows us to measure the work  $W$  during the resulting fast unfolding and refolding processes within Monte Carlo simulations, i.e., in nonequilibrium. Also we sample numerically efficiently directly in exact equilibrium, for comparison. Using a sophisticated large-deviation algorithm, we are able to measure work distributions with high precision down to probabilities as small as  $10^{-46}$ , enabling us to verify the Crooks and Jarzynski theorems. Furthermore, we analyze force-extension curves and the configurations of the secondary structures during unfolding and refolding for typical equilibrium processes and nonequilibrated processes. We find that the nonequilibrated processes where the work values are close to those which are most relevant for applying Crooks and Jarzynski theorems, respectively, but which occur with exponential small probabilities, are most and quite similar to the equilibrium processes.

DOI: [10.1103/PhysRevE.104.034407](https://doi.org/10.1103/PhysRevE.104.034407)**I. INTRODUCTION**

In statistical physics, the modeling of equilibrium systems is well understood [1]. Nevertheless, due to open system boundaries, or system driving or the lack of infinite time to perform experiments or simulations, most real and simulated model systems are constantly in nonequilibrium. The theoretical treatment of nonequilibrium systems is more challenging as compared to the equilibrium case. Still, relations between equilibrium and nonequilibrium appear for many occasions, like aging in glassy systems [2], or for the Mpemba effect where sometimes hot water cools faster than cold water [3]. A particularly illuminating bridge between both worlds is provided by the theorems of Jarzynski [4] and Crooks [5]. There and in the present work, systems are considered which are in contact to a heat bath, thus subject to thermal fluctuations, i.e., the systems have a stochastic nature. The dynamics of the systems may be deterministic or stochastic as well. Also, the systems are subject to a change of an external parameter. Typically the considered speed of the parameter change is fast as compared to the system equilibration times. For this reason the such considered processes are termed nonequilibrated. Note that the parameter changes usually lead to physical work performed on the system. The stochastic nature of the system results in a distribution  $P(W)$  of work  $W$ . Since any parameter change may be reversed, there exist a corresponding distribution  $P_{\text{rev}}(W)$  for the reverse process. For a system coupled to a heat bath, the Crooks theorem reads  $P(W) =$

$P_{\text{rev}}(-W) \exp(-(\Delta F - W)/T)$ . This can be used to reconstruct the true free energy difference  $\Delta F$  between initial and final state, because  $P(W)$  and  $P_{\text{rev}}(-W)$  cross at  $W = \Delta F$ . Analogously the Jarzynski equation reads  $\langle e^{-W/T} \rangle = e^{-\Delta F/T}$ . These and related theorems have led to many applications and extensions relating equilibrium and nonequilibrium processes in a field called *stochastic thermodynamics* [6–13]. One fruitful field of applications is biophysics, where these theorems are used to measure properties of small molecules like RNA.

One major goal of stochastic thermodynamics is to extract equilibrium information from nonequilibrium measurements or simulations [14]. The fluctuation theorems concern specific measurable scalar quantities like work [4,5,15], entropy [16–24], or a quantity measuring the volume of the phase space [25]. However, beyond statistics of particular scalar quantities, the fluctuation theorems do not provide information about the behavior along a corresponding equilibrated trajectory, i.e., with respect to arbitrary measurable quantities or possibly full configurations. Here “equilibrated” means either that between measurements, e.g., recording of a configuration, the system is given enough time to relax. On the other hand, as is the case here, a direct equilibrium sample may technically be possible.

Now, standard derivations of the fluctuations theorems involve only terms which include energies and probabilities of the initial and final state. What may we expect when we analyze the full trajectory of a nonequilibrated process? First, a *typical*, i.e., highly probable sample of a nonequilibrated

trajectory will look very different from a corresponding trajectory sampled during an equilibrium process. Second, it is known that when reweighting trajectories suitably in a time-dependent way, they also carry some information about the intermediate equilibrium states, at the corresponding intermediate values of the control parameter [24,26,27]. This allows for the reconstruction of full free-energy profiles beyond initial and final state. Third, it is somehow intuitive to believe that the *rare* nonequilibrated processes which contribute most to the estimation of  $\Delta F$  are in a comprehensive way, without reweighting, similar or even equal to the corresponding equilibrium processes. For the case of the Crooks and Jarzynski theorems, the statistics of the work distributions are most relevant for particular work values  $W = \Delta F$  and  $W = W_j^*$ , where the latter one is the value where the integrand  $e^{-W/T} P(W)$  exhibits a maximum. Note that these values are highly improbable to occur for large system sizes. Thus, rare events may play a major role in the understanding of nonequilibrated or nonequilibrium processes in general and in the application of work theorems.

This motivates our present work: We investigate in a comprehensive way the dynamics of nonequilibrated processes for a system coupled to a heat bath. We consider a large range of nonequilibrium work values  $W$ , the typical regions as well as those for rare untypical values of  $W$ . Then we select trajectories according their value of  $W$ , typical and rare ones, and compare with the equilibrium process behavior.

For this purpose we want to study a model which exhibits at low temperatures a complex low-temperature phase with a nontrivial energy landscape, possibly allowing for quenched-disorder ensembles. This leads to slow glasslike dynamics which makes it hard to reach equilibrium for such a model. Furthermore, the model should include the possibility of performing external work in nonequilibrium and, at the same time, it should allow for an efficient sampling of configurations in equilibrium, for comparison. A natural candidate and often used for fundamental studies in statistical mechanics is the Ising model [28], but, unfortunately, it does not allow for exact sampling, unless the behavior of the model is too simple. Therefore, we have chosen another model which meets the above criteria, i.e., the unfolding and refolding of RNA secondary structures subject to an external force [29]. The former one, denoted as *forward* process, involves stretching an RNA by subjecting it to an external force  $f$  which is increased from starting at zero. For the latter one, denoted as *reverse* process, one starts with a large force and reduces it to zero. For small RNAs consisting of few dozens of bases, the Crooks theorem has been confirmed in experiments [30,31] and simulations [15,32] for slow unfolding and refolding processes. For such small RNA and slow processes, the resulting work distributions are rather broad and the distribution for forward and reverse processes are close to each other such that they cross at high-probability values which are easily accessible. For larger RNA molecules, the crossing points will move to smaller probabilities, such that the crossing can not be observed in experiments or standard simulations. To go beyond such limiting system sizes, we applied for our study sophisticated large-deviation algorithms [33,34]. This allows one to measure probability distributions numerically down to extremely small probabilities. These algorithms have also

been applied successfully to nonequilibrium processes like the transition-path sampling approach to study protein folding [35,36], population-based approaches to study asymmetric exclusion processes [37,38] or Markov-chain Monte Carlo (MC) methods to investigate, e.g., traffic models [39] and the Kardar-Parisi-Zhang equation [40]. In particular such an algorithm has also been used to measure with high precision the work distribution of an Ising model subject to a varying external field [41], providing the first confirmation of the Jarzynski and Crooks theorems for a large system with many thousands of particles.

Thus, here we will provide similar evidence for RNA secondary structure unfolding and refolding by applying such a MC rare-event algorithm. The MC algorithm works in the space of the random numbers which drives the underlying dynamics and applies biases which direct the MC sampling to possibly rare values of the work. This allows us to obtain the work distributions of intermediate-sized RNAs down to probabilities as small as  $10^{-46}$ . Furthermore, we will analyze the temporal structure of the nonequilibrated processes, selected by the occurring work values  $W$ . We will compare this to the corresponding equilibrium process, which can be sampled exactly [42–44] and efficiently, i.e., in polynomial time, for RNA secondary structures without pseudoknots. Beyond confirming the Jarzynski and Crooks theorems we find in particular that the nonequilibrated processes can be very similar in their development to the equilibrium ones. The highest similarity is reached for processes which exhibit a work value  $W$  between the values  $W = \Delta F$  and  $W = W_j^*$  which are most relevant for the Crooks and the Jarzynski theorem, respectively.

We will next present our model and the used simulation methods. Then we show our results and finish by a discussion.

## II. MODEL

Each RNA molecule is a linear chain  $\mathcal{R} = (r_i)_{i=1,\dots,L}$  of bases, also called residues, with  $r_i \in \{A, C, G, U\}$  and  $L$  is the length of the sequence. For a given sequence  $\mathcal{R}$  of bases, a *secondary structure* is a set of pairs of bases, such that for the present simple model only *complementary* (Watson-Crick) base pairs A-U and C-G are allowed. This can be described by a set  $\mathcal{S}$  of pairs  $(i, j)$  (with the convention  $1 \leq i < j \leq L$ ), meaning that bases  $r_i$  and  $r_j$  are paired. For convenience, we also use  $s(i) = j$  if  $i$  is paired to  $j$ , which implies  $s(j) = i$ , and  $s(i) = 0$  if  $i$  is not paired. Our restriction to Watson-Crick pairs means for A-U either  $r_i = A$  and  $r_j = U$  or vice versa, correspondingly for the C-G pair. Note that the chain of residues corresponds to a one-dimensional system. Since pairs between arbitrary strutures are allowed, the secondary structure model is in some sense a mean-field model.

Still the model describes the behavior of real three-dimensional molecules, which leads, in a simplified way, to the following two additional restrictions: (1) We exclude so-called *pseudoknots*, which means, for any  $(i, j), (i', j') \in \mathcal{S}$  with  $i < i'$ , either  $i < j < i' < j'$  or  $i < i' < j' < j$  must hold. In the first case, pair  $(i, j)$  is located entirely before  $(i', j')$  in the sequence. In the second case, pair  $(i', j')$  is called to be *inside* of  $(i, j)$ . If a bond is not inside of any other bonds, we say it occurs on the *first level*, i.e., it is the topmost pair of the structure enclosing all other pairs. Neglecting pseudoknots

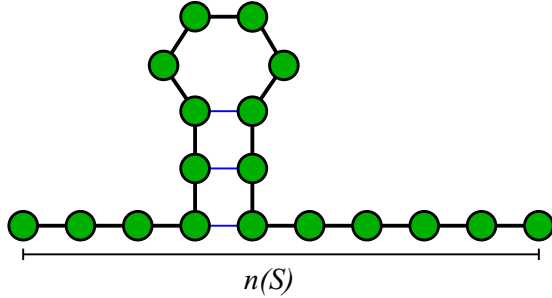


FIG. 1. An example for a RNA secondary structure with one globule and a line indicating the extension  $n(S)$  of the folded RNA. Circles denote bases, thick black lines links between consecutive bases, and thin blue lines hydrogen bonds between complementary bases.

follows the notion of them being more an element of the tertiary structure [45]. It also means that it is always possible to draw the molecule as a single line and connect all pairs by lines such that no intersections occur. (2) Due to the bending rigidity of the molecule, between two paired bases a minimum distance is required, i.e.,  $|j - i| > s$ .

Every secondary structure  $\mathcal{S}$  is assigned a certain energy  $E(S)$ , where the dependency on the sequence  $\mathcal{R}$  is not explicitly indicated. This energy is defined by assigning each pair  $(i, j)$  a certain energy  $e(r_i, r_j)$  depending only on the kind of bases.

Furthermore there is a contribution arising from the external force  $f$  which stretches the chain to its extension  $n = n(S)$ , as introduced previously [29]. The extension of the structure is the part of the RNA which is outside any paired base, plus length 2 for any paired base on the first level. Hence, any globule in the chain contributes two length units. This is illustrated in Fig. 1. This interaction with the external force  $f$  gives rise to an energy contribution  $-f \times n$ .

The total energy for the most basic model is the sum over all pairs plus the interaction with the external force

$$E(S) = \sum_{(i,j) \in \mathcal{S}} e(r_i, r_j) - n(S)f. \quad (1)$$

By choosing  $e(r, r') = +\infty$  for noncomplementary bases  $r$  and  $r'$ , pairings of this kind are suppressed. Here we use the most simple energy model, i.e.,  $e(r, r') = -1$  for complementary bases A-U and C-G. Note that in this simple form our model can also be seen as a model for single-stranded DNA. Note that the purpose of this study is a fundamental statistical mechanics one, to investigate the relationship between equilibrium and rare nonequilibrium behavior. Therefore, the model we use is at the same time simple enough but also sophisticated enough. When on the other hand someone aims at modeling real RNA as realistically as possible, one would have to use an even more comprehensive model. For such cases, stacking energies have to be included and also, when it comes to free energy calculations, entropic effects related to steric constraints that are originating from different types of loops and multiloops. Software packages like *mfold* [46], *Sfold* [47], *RNAstructure* [48], or the *Vienna RNA Package* [44] exist for such detailed modeling with a biophysics focus.

### III. ALGORITHMS

In the following, we discuss the algorithms we have used. First, we show how RNA secondary structures can be sampled directly in equilibrium. For the nonequilibrium folding and unfolding simulations, our dynamics consist of single base pair steps performed within Markov chain MC simulations of RNA structures, as presented in the second subsection. Thus, one time unit of the simulation is one MC sweep. To study rare unfolding and folding trajectories, we used a second type of MC simulations, which is wrapped around the RNA MC simulations, as presented in the third subsection.

#### A. Sampling secondary structures

For RNA secondary structures it is possible to sample them directly in equilibrium for finite temperatures  $T$  in time  $O(L^3)$ . We used an extension of the approach for the zero-force case [42]. For this purpose, one needs also to calculate partition functions for some subsequences, which is possible using *dynamic programming* in polynomial time. These approaches [29,49] are also extensions of the zero-force case method [50].

The partition function  $Z_{i,j}$  ( $i \leq j$ ) for subsequence  $r_i \dots r_j$  at inverse temperature  $\beta = 1/T$  without external force and without length constraints, obeying the minimum distance  $s$  between two paired bases, is given by

$$\begin{aligned} Z_{i,j} &= 1 && \text{for } j - i \leq s, \\ Z_{i,j} &= Z_{i,j-1} \\ &+ \sum_{k=i}^{j-s-1} Z_{i,k-1} e^{-\beta e(r_k, r_j)} Z_{k+1, j-1} && \text{else.} \end{aligned} \quad (2)$$

All  $O(L^2)$  values of  $Z_{i,j}$  can be conveniently calculated [50] by a *dynamic programming approach*, i.e., starting with  $Z_{i,i}$  and continuing with increasing values of  $j - i$ . Since most contributions involve a sum of  $O(L)$  terms, the algorithm has a running time of  $O(L^3)$ .

In order to include the interaction with the external force, one needs additionally the partition function  $Q_{1,j,n}$  of the subsequence  $r_1, \dots, r_j$  such that the extension is fixed to the value  $n$ , with  $n \leq j$ . We include the fixed index 1 for matching with the notation for  $Z_{i,j}$ ,

Our approach follows the lines of corresponding methods [29,49] for calculation of partition functions and ground state energies of RNA secondary structures subject to an external force. The partition function reads

$$\begin{aligned} Q_{1,1,1} &= 1, \\ Q_{1,j,1} &= 0 && \text{for } j > 1, \\ Q_{1,2,2} &= Z_{1,2}, \\ Q_{1,j,2} &= 0 && \text{for } 2 < j \leq s + 1, \\ Q_{1,j,2} &= e^{-\beta e(r_1, r_j)} Z_{2,j-1} && \text{for } j > s + 1, \\ Q_{1,j,n} &= Q_{1,j-1,n-1} \\ &+ \sum_{k=n-1}^{j-s-1} Q_{1,k-1,n-2} e^{-\beta e(r_k, r_j)} Z_{k+1, j-1} \end{aligned}$$

$$\text{for } n > 2, j \geq n. \quad (3)$$

Also all these partition functions can be conveniently calculated by dynamic programming in time  $O(L^3)$ .

This allows us to calculate the partition function with force for subsequence  $r_1, \dots, r_j$  by

$$\tilde{Z}_{1,j}(f) = \sum_{n=1}^j Q_{1,j,n} e^{\beta n f}. \quad (4)$$

Note that the case  $n = 0$  can not occur and the case  $n = 1$  corresponds only to one single base. With this it is possible to calculate the mean extension of an equilibrium structure at force  $f$  with

$$\bar{n}_{Eq}(f) = \sum_{n=1}^L n Q_{1,L,n} e^{\beta n f}. \quad (5)$$

The availability of the above partition functions also allows us to sample secondary structures in the presence of an external force directly, i.e., rejection free, also in polynomial time. The approach is an extension of the zero-force algorithm [42] to the case  $f \geq 0$ .

For sampling a structure, the following probabilities are needed. The probability  $p_{i,j,k}^p$  that for subsequence  $r_i, \dots, r_j$ , without the presence or influence of a force, base  $j$  is paired to base  $k$  with  $i \leq k < j$  and  $j - k > s$  is given by

$$p_{i,j,k}^p = \frac{Z_{i,k-1} e^{-\beta e(r_k, r_j)} Z_{k+1, j-1}}{Z_{i,j}}. \quad (6)$$

For  $j - k \leq s$ , this probability is zero. The probability that base  $j$  is not paired is given by

$$p_{i,j}^u = \frac{Z_{i, j-1}}{Z_{i,j}}. \quad (7)$$

The probability  $\tilde{p}_{1,j,k}^p(f)$  that for subsequence  $r_1, \dots, r_j$ , with the presence of a force  $f$ , base  $j$  is paired to base  $k$  with  $1 \leq k < j$  and  $j - k > s$  is given by

$$\tilde{p}_{1,j,k}^p(f) = \frac{\tilde{Z}_{1, k-1}(f) e^{-\beta e(r_k, r_j) + \beta 2f} Z_{k+1, j-1}}{\tilde{Z}_{1,j}(f)}. \quad (8)$$

For  $j - k \leq s$ , this probability is zero. The probability that base  $j$  is not paired is given by

$$\tilde{p}_{1,j}^u(f) = \frac{\tilde{Z}_{1, j-1}(f) e^{\beta f}}{\tilde{Z}_{1,j}(f)}. \quad (9)$$

The sampling of a structure is now performed as follows. Each time one starts for the full sequence  $r_1, \dots, r_L$  by considering the *case with force*  $f$ :

(1) *Case with force*  $f$  for subsequence  $r_1, \dots, r_j$ :

Base  $j$  is paired to one of the bases  $k = 1, \dots, j - s - 1$  with probability  $\tilde{p}_{1,j,k}^p(f)$ , respectively, and remains unpaired with probability  $\tilde{p}_{1,j}^u(f)$ .

Now, if base  $j$  has been paired to base  $k$ , recursively the sequence  $r_1, \dots, r_{k-1}$  is treated in the same way (*case with force*  $f$ ) and the subsequence  $r_{k+1}, \dots, r_{j-1}$  is treated as described in the *case without force*.

If base  $j$  has not been paired, the sequence  $r_1, \dots, r_{j-1}$  is treated in the same way (*case with force*  $f$ ).

(2) *Case without force* for subsequence  $r_i, \dots, r_j$ :

Base  $j$  is paired to one of the bases  $k = i, \dots, j - s - 1$  with probability  $p_{i,j,k}^p$ , respectively, and remains unpaired with probability  $p_{i,j}^u$ .

Now, if base  $j$  has been paired to base  $k$ , recursively the sequence  $r_i, \dots, r_{k-1}$  and  $r_{k+1}, \dots, r_{j-1}$  are treated in the same way (*case without force*).

If base  $j$  has not been paired, the sequence  $r_i, \dots, r_{j-1}$  is treated in the same way (*case without force*).

In this way, each time a structure is independently drawn according to the Boltzmann distribution, i.e., the algorithm constitutes ideal sampling.

When we sample a folding or an unfolding trajectory in equilibrium, i.e., for a sequence of force values  $f_k = f_0 + k\Delta f$  ( $k = 0, 1, 2, \dots$ ), we just sample an equilibrium structure  $\mathcal{S}_k$  for all force values  $\{f_k\}$  encountered. This we call equilibrium trajectory or, more generally, an equilibrium process. Here we use  $f_k \in [0, 2]$  and 400 different force values, i.e.,  $\Delta f = \pm 0.005$ . To each trajectory a work of  $W = -\sum_k n(\mathcal{S}_k)\Delta f$  is associated. This corresponds to a small force increment and a subsequent imaginary (infinite) long waiting time, either in real time or in terms of MC or molecular dynamic steps when performing simulations, until the next equilibrium structure is encountered. Since we use very small force increments, the work we measure is actually numerically very close to  $\Delta F$ , as we have verified.

## B. Folding and unfolding algorithm

The algorithm for performing an unfolding or refolding process in nonequilibrium, and to measure the performed work  $W$  for a given sequence  $\mathcal{R}$ , works as follows: First, an initial secondary structure  $\mathcal{S}$  is drawn in equilibrium at some given initial value  $f_0$  of the force and for RNA temperature  $T$ . Then a Markov chain MC simulation is performed, called *RNA MC* here. Here we use discrete time steps for convenience and specify below the transition probabilities we use. But also continuous-time MC methods are used to simulate the dynamics of physical processes, in which case the algorithms are often called *kinetic MC* [51], and one would specify transition rates instead. The RNA MC is allowed to perform *small* changes of the secondary structure, usually called *local* moves in the MC literature. As we detail below, the changes are closing and opening of single base pairs. A total of  $n_{MC}$  sweeps is performed while the force parameter  $f$  is increased or reduced depending on  $\Delta f$ . Note that the dynamics within Monte Carlo does not correspond to solving Newton's equations of motion, which are not available for this discrete model anyway, but describe effective physical dynamics, e.g., of a system coupled to a heat bath. It is widely used, e.g., for simulation of dynamics in Ising systems, where MC dynamics can be actually derived from quantum mechanics [52]. Also, e.g., diffusion processes, chemical reactions, polymer dynamics or surface growth are often investigated using MC simulations, even if a microscopic classical or quantum model is available, just for the purpose of accessing large-enough timescales. In particular, due to the small changes performed in the MC approach, a sweep actually corresponds to a physical timescale [53], which is larger than the one describing the smallest microscopic movements. For most investigations, also the one presented here, it is not necessary to know the exact timescale of one MC step, but for some models the mapping is interestingly known. For example, for Ising spin glasses, one MC sweep of a single-spin flip update algorithm corresponds

roughly to one picosecond [54]. But also for the MC approach to RNA folding, estimates of the conversion factor between MC step and time exist, for a hairpin structure it was found that one MC step correspond roughly to  $1.2 \times 10^{-7}$ s [55].

For the unfolding process, we used  $f_0 = 0$  and increased the force until  $f = 2$  was reached, while for the refolding process we started at  $f_0 = 2$  and decreased the force to  $f = 0$ . During the RNA MC simulation,  $n_{\text{force}}$  times the force is increased by  $\Delta f$ . Each time the force is changed, we obtained a contribution  $\Delta W = -n(\mathcal{S})\Delta f$  to the work, where  $n(\mathcal{S})$  is the current extension.

The MC sweeps allow for the influence of thermal fluctuations. Since the number of possible Watson-Crick pairs is  $O(L^2)$ , we define one sweep as  $L^2/2$  MC steps. For the individual MC steps, each time two random residues  $i$  and  $j$  are selected. If these are already paired to each other in the current structure  $\mathcal{S}$ , a trial configuration  $\mathcal{S}'$  is made by removing the pair, i.e., the bond is broken. In case of two nonbonded bases, they will be paired in the trial configuration  $\mathcal{S}'$  if they are complementary, and if they have a distance larger than  $s$ , and if no pseudoknots would be created. The configuration is not changed when just one of the selected bases is already bounded, since a base can connect only to a single other one. For these cases, the trial configuration is accepted, i.e., becomes the current one, with the usual Metropolis probability  $p_{\text{Metr}} = \min\{1, \exp(-\beta\Delta E)\}$  determined by the energy change  $\Delta E = E(\mathcal{S}') - E(\mathcal{S})$ . The random numbers which are used during the RNA MC simulation are generated before a call to the subroutine and stored in a vector  $\xi$ . In this way, all the randomness is removed outside this subroutine [56], for a reason we will present in the next section. Note that all other parameters like  $\mathcal{R}$ ,  $T$  etc. remain the same during a simulation, thus the work obtained during unfolding or refolding is a deterministic function of  $\xi$ :

---



---

**algorithm**  $W(\xi)$

**begin**

draw for  $\mathcal{R}$  an equilibrium structure  $\mathcal{S}$  at  
initial force  $f_0$  and RNA temperature  $T$

$f = f_0$

$W = 0$

**for**  $j = 0, \dots, n_{\text{force}}$

**begin**

perform  $L^2 n_{\text{MC}} / (2 n_{\text{force}})$  MC steps:

**begin**

select two random residues  $l, m \in \{1, \dots, L\}$

**if**  $(l, m) \in \mathcal{S}$ , remove pair with prob.  $p_{\text{Metr}}$ .

**else if**  $(l, m)$  is allowed set  $\mathcal{S} = \mathcal{S} \cup \{(l, m)\}$   
with prob.  $p_{\text{Metr}}$ .

**end**

$f = f + \Delta f$

$W = W - n(\mathcal{S})\Delta f$

**end**

**return** ( $W$ )

**end**

---



---

The vector  $\xi = (\xi_1, \xi_2, \dots, \xi_K)$  contains  $K = L - 1 + 3L^2 n_{\text{MC}} / 2$  random numbers which are uniformly distributed

in  $[0, 1]$ . These are all random numbers that are needed to perform one full unfolding or refolding simulation. Each random number has a specific fixed purpose. The first  $L - 1$  entries are required to sample an configuration from the partition function, where an individual random number is utilized to determine if base  $j \in [2, \dots, L]$  is either connected to base  $k \in [1, \dots, j - s - 1]$  or unconnected. Not all of these  $L - 1$  random numbers are necessarily used during a specific sampling process, e.g., if for base  $j$  the remaining subsequence for a potential pairing partner is too small. In this case, the corresponding random number is just ignored, The subsequent MC steps need three random numbers each, two for selecting a pair and potentially one more, if the Metropolis criterion is used. If not, the third random number is also ignored, respectively. This results in a number of  $3L^2 n_{\text{MC}} / 2$  additional entries in  $\xi$ .

Note that more efficient MC algorithms for RNA secondary structures exists [57,58], which are event-driven Gillespie algorithms. Also they take as possible MC moves only allowed moves into account, i.e., either pairs are removed, or only allowed pairs are proposed, avoiding non-complementary base pairs or pseudoknots. This requires keeping track of the allowed moves, which also generates quite some overhead in computation and it also involves the calculation of necessary corrections factors due to the varying number of accessible neighboring secondary structure configurations, in order to guarantee detailed balance. Also, the Gillespie nature of these algorithms make the use of random numbers dependent on the history of previous events. Nevertheless, for the present application, the work process is embedded into another higher-level MC simulation; see below. For a good performance of the higher-level MC simulation this requires that for each entry of the vector a specific purpose is assigned, as presented above. If this requirement is met, small changes to  $\xi$  yield typically small, i.e., not too ‘‘chaotic’’ changes in the resulting work  $W = W(\xi)$ . This is the case with the present algorithm.

### C. Large-deviation approach

By repeating an unfolding or refolding simulation many times, one can measure approximately the work distributions  $P(W)$  and  $P_{\text{rev}}(W)$ , respectively. Nevertheless, this *simple sampling approach* allows one to obtain the work distributions only down to rather large probabilities, like  $10^{-9}$ . To obtain the work distributions down to much smaller probabilities, we applied sophisticated large-deviation algorithms [33,34]. Our approach has already been used to measure work distributions for large Ising systems [41]. The basic idea is to drive the forward and reverse processes, respectively, by vectors  $\xi$  of random numbers and control the composition of the vectors with a Markov chain MC simulation, with a known, i.e., removable, bias depending on the measured work.

As mentioned in the previous section, for a given sequence  $\mathcal{R}$ , temperature  $T$  and the other parameters, which are all kept fixed for a set of simulations, the outcome of the unfolding or refolding process is solely determined by the random values contained in the vector  $\xi$ . Thus, to perform a standard *simple sampling* simulation, each time a random vector  $\xi$  is drawn with all its entries being a pseudo random number uniformly

distributed in  $[0,1]$ . This results in one work value  $W$  which is sampled from the true distribution. Thus, if one repeats the simple sampling many times, one can collect many work values and calculate a histogram to approximate the full distribution. Nevertheless, running the simple sampling  $K$  times will allow one only to resolve probabilities larger or equal to  $1/K$  in the histogram.

In order to access the work distribution down to very small probabilities, the following is done: Another Markov chain MC simulation is employed, where the states of the simulation are represented by samples  $\xi^{(t)}$  of the random vectors that drive the RNA unfolding or folding simulations. Thus, each state of the Markov chain corresponds to exactly one instance of a full RNA MC process consisting of starting with an initial state in equilibrium and performing a, typically fast, nonequilibrated process during which the force is changed. “Fast” means here that the system is allowed only for a couple of RNA MC steps to relax between two force changes, respectively. In the end, a work value  $W = W(\xi^{(t)})$  is obtained. Therefore, the MC simulation takes place on a higher level than the unfolding or refolding RNA MC simulations. Now, the main idea is to include a bias in the high-level MC simulation, which involves a Metropolis acceptance depending on the change in the resulting work.

To be more precise, say we have the current state  $\xi^{(t)}$  with work  $W^{(t)} = W(\xi^{(t)})$  in the MC simulation. First, a *trial state*  $\xi'$  is generated, by copying  $\xi^{(t)}$  and then redrawing a number  $n_\xi < K$  of randomly selected entries from the  $K$  entries of  $\xi'$ . Next, a complete work process is performed for  $\xi'$ , which results in the measured work  $W' = W(\xi')$ . The trial state is then accepted, i.e.,  $\xi^{(t+1)} = \xi'$  with Metropolis probability  $\tilde{p}_{\text{Metr}} = \min\{1, \exp(-\Delta W/\Theta)\}$ , where  $\Delta W = W' - W^{(t)}$  is the change in work and  $\Theta$  is a temperature-like control parameter. Otherwise, the trial state is rejected, i.e.,  $\xi^{(t+1)} = \xi^{(t)}$ . Note that an empirical acceptance rate of around 0.5 is aimed for, such that  $n_\xi$  is typically small for small values of  $\Theta$  and larger for larger values of  $\Theta$ . Actual values are given below.

Since the setup of the high-level MC simulation is like any standard MC approach for a system coupled to a heat bath, only that the energy is replaced by the work and  $\Theta$  is used for the temperature, it is obvious that our approach will sample the true work distribution but including a bias which is exactly the Boltzmann factor  $\sim \exp(-W/\Theta)$ . As usual, the initial phase of the Markov chain, i.e., the equilibration phase, is discarded and sample values are drawn only at suitable large MC time intervals. Thus, one can in principle perform simulations for a given value of  $\Theta$ , measure a histogram approximating the biased distribution  $P_\Theta(W) \sim P(W) \exp(-W/\Theta)$  and obtain an estimate for the true distribution  $P(W)$  by multiplication with  $\exp(+W/\Theta)$ , up to a normalization constant. Note that, technically, to resolve the distribution over a large range of the support, one needs to perform simulations at several suitably chosen values of the control temperature  $\Theta$ , get the normalization constants for all measured histograms and combine them into one single finally normalized histogram [33]. Details, in particular for the case of the work distribution of on Ising model in an external field, can be found elsewhere [41]. This approach has already been applied to other nonequilibrium processes like the Kardar-Parisi-Zhang model [40] or traffic flows [39].

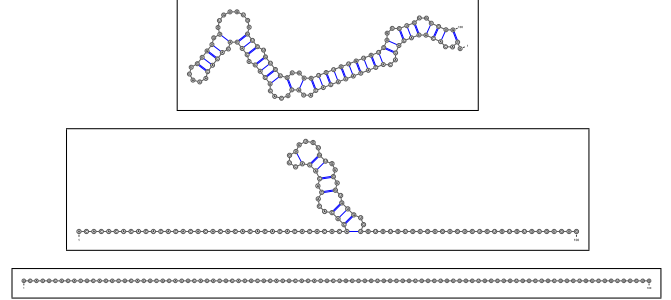


FIG. 2. Exemplary equilibrium secondary structures at  $T = 1$  for different forces. Top:  $f = 0$ . Middle:  $f = 0.805$ . Bottom:  $f = 2$ . Drawn with the VARNA package [59].

Note finally, that if one aims at using a more realistic (free) energy model for the RNA calculations, it would not be possible to just use existing packages like *mfold* [46], *Sfold* [47], *RNAstructure* [48], or the *Vienna RNA Package* [44] because they use random number generators internally and do not allow for feeding in vectors  $\xi$  of numbers to be used.

#### IV. RESULTS

An RNA sequence is considered, which is not too small, such that differences between equilibrium and nonequilibrium secondary structure configurations can be observed with suitable resolution. Concretely, we studied a hairpin structure of length  $L = 100$  which has the sequence  $(AC)^{25}(UG)^{25}$ , resulting in a ground state of one large stack with a small loop. This sequence is chosen because hairpins are common secondary structure elements of RNA, which have been studied frequently experimentally not only in thermal equilibrium [60], but also in direct use to verify the Crooks theorem and the Jarzynski relation [30,31] by folding and unfolding hairpins by mechanical force. Hairpins are likewise used in simulations that aim to reproduce experimental results [32,61]. Also numerically, an exponential increase of the unfolding MC time with the hairpin stem length was observed, while the folding MC time is almost independent of stem and loop length [55]. This shows that the thermodynamic behavior can be complex, making it an ideal candidate for our study. On the other hand, the fluctuations in force-extension curves decrease with the number of hairpins in the overall secondary structure, due to a compensation effect [49]. Finally and interestingly, due to its simple structure, there even exists an analytical solution of the partition function in the limit of large  $L$  for a hairpin structure [62].

For the studied RNA size of  $L = 100$ , the application of large-deviation algorithm is necessary to measure the work distribution with suitable accuracy such that the Jarzynski and Crooks theorems can be applied and the unfolding and refolding histories can be captured.

We considered the RNA to be coupled to a heat bath at temperatures  $T = 0.3$  and  $T = 1$ , respectively. These are low enough temperatures, such that in the force-free case, the RNA is basically folded, but exhibits thermal fluctuations. Example equilibrium secondary structures are shown in Fig. 2. It becomes apparent how the extension increases with the force parameter  $f$ .

TABLE I. Simulation parameters for different temperatures  $T$ , for different process speeds  $n_{MC}$  and unfolding ( $f = 0 \rightarrow 2$ ) and refolding ( $f = 2 \rightarrow 0$ ) processes. For the high-level MC simulation  $n_{\Theta}$  different values of the temperature-like parameter  $\Theta \in [\Theta_{\min}, \Theta_{\max}]$  were considered. In each MC step a number  $n_{\xi} \in [n_{\xi,\min}, n_{\xi,\max}]$  of entries from the vectors  $\xi$  of random numbers are changed. For the lowest value of  $\Theta$  we have  $n_{\xi} = n_{\xi,\min}$ , for the largest  $n_{\xi} = n_{\xi,\max}$ , for the others in between. The total number of MC steps in the large-deviation simulation was always larger than the given values  $t_{ld}$ , the actual values depending on the value of  $\Theta$  and on the available computing time on the computing cluster, respectively. The longest running time occurred for the unfolding (forward) process  $T = 1$ ,  $n_{MC} = 8$  and took  $t_{ld} = 14.5 \times 10^8$  steps.

$T$	$n_{MC}$	$f$	$n_{\Theta}$	$\Theta_{\min}$	$\Theta_{\max}$	$n_{\xi,\min}$	$n_{\xi,\max}$	$t_{ld}/10^8$
0.3	8	$0 \rightarrow 2$	17	0.6	7	938	$9 \times 10^4$	5.44
0.3	8	$2 \rightarrow 0$	10	0.4	2	1587	$6 \times 10^4$	4.05
0.3	16	$0 \rightarrow 2$	18	0.6	8	1407	$12 \times 10^4$	2.50
0.3	16	$2 \rightarrow 0$	10	0.457	2	2557	$9 \times 10^4$	1.82
1	8	$0 \rightarrow 2$	11	0.8	10	354	$6 \times 10^4$	6.95
1	8	$2 \rightarrow 0$	13	1	5	1350	$6 \times 10^4$	2.81
1	16	$0 \rightarrow 2$	11	0.8	10	938	$75 \times 10^2$	4.41
1	16	$2 \rightarrow 0$	10	0.8	5	2344	$12 \times 10^4$	2.35

For all unfolding and refolding processes, the force was increased from  $f_0 = 0$  to  $f_{\max} = 2$  and vice versa, with 400 steps each. Thus, the change of the force was  $\Delta f = \pm 0.005$ . Two different speeds of the processes were simulated, i.e., two different numbers  $n_{MC}$  of sweeps performed during the process, here  $n_{MC} = 8$  and  $n_{MC} = 16$ . This can be compared to typical MC timescales needed to equilibrate RNA secondary structures of the hairpin using the RNA MC approach, while beginning from an empty structure. We performed some tests and found that for  $T = 1$  and  $f = 0$  the hairpin structure finds typical configurations (as measured by the overlap, see Sec. IV C) in about 1000 sweeps while for  $T = 0.3$  it takes roughly 40 000 sweeps. Thus, our nonequilibrated processes are fast compared to the equilibration MC time. Table I shows the other simulation parameters we have used.

### A. Work distributions

In Fig. 3 the work distributions  $P(W)$  of the forward and  $P_{\text{rev}}(-W)$  of the reverse processes are shown for the case  $T = 1$  and  $n_{MC} = 16$ . With the application of the large-deviation scheme, very small probabilities down to  $10^{-26}$  could be resolved, i.e., over 26 orders in magnitude. The crossing of the distributions at a work value  $W = \Delta F$  predicted by the theorem of Crooks [5] can be well observed. For the present model, because the partition function can be calculated exactly numerically, we are able to obtain  $\Delta F = 1/T \log\{Z(f = f_0)/Z(f = f_{\max})\}$ . Apparently, the data matches the expectations from the Crooks theorem with high precision.

The Crooks relation means that when  $P_{\text{rev}}(-W)$  is rescaled according the exponential  $\exp(-(\Delta F - W)/T)$ , it equals  $P(W)$ . This is also confirmed very convincingly by our data over up to 15 decades, as shown in the inset of Fig. 3. This in particular shows that our higher-level MC simulation is well

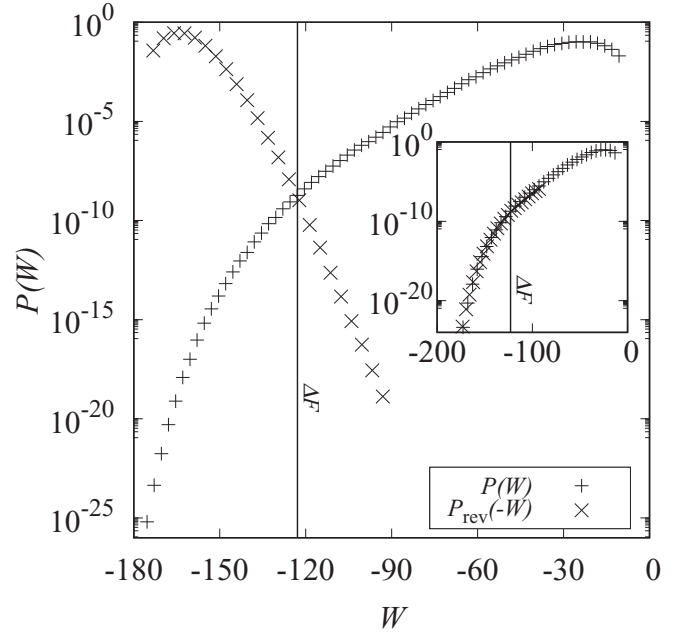


FIG. 3. Plain and mirrored work distributions for  $T = 1$  and 16 sweeps of the forward and reverse process, respectively. They intersect near  $W = \Delta F$ , which is the exact value and indicated by the vertical line. The inset shows the same plot but with the distribution for the reverse process (cross symbols) rescaled as  $P_{\text{rev}}(-W) \exp(-(\Delta F - W)/T)$ , according to the Crooks equation, yielding a good agreement with  $P(W)$ .

equilibrated [41]. Similar results were obtained for the faster  $n_{MC} = 8$  process (not shown).

In Fig. 4 the corresponding results for the lower temperature  $T = 0.3$  ( $n_{MC} = 16$ ) are shown. Again, the Crooks theorem is confirmed with high precision. For the case  $n_{MC} = 8$  (not shown) the distribution even reaches probabilities as small as  $10^{-46}$ .

### B. Jarzynski integrand

The integrand of  $\langle e^{-W/T} \rangle = \int dW P(W) e^{-W/T}$  is shown in Fig. 5, for  $T = 1$ ,  $n_{MC} = 8$  and forward and reverse work processes, respectively. The point where the integrand peaks is exponentially relevant and can be used to approximate the integral. Here this is the value  $W_j^* \approx -172$ . This, together with its probability, determines according to the Jarzynski equation the free energy difference via  $P(W_j^*) e^{-W_j^*/T} \approx e^{-\Delta F/T}$ , i.e.,  $\Delta F = W_j^* - T \log P(W_j^*)$ , which explains the notable difference of  $W_j^*$  from  $\Delta F$ .

### C. Similarity to equilibrium

Our results allow us to go beyond calculation of distributions and study the actual dynamic processes. This is in particular possible when selecting among all sampled trajectories any value of  $W$ . We concentrate now on  $T = 1$ , the results for  $T = 0.3$  are similar. During a forced process, we sampled structures, one for each considered value of  $f$ , in equilibrium and in nonequilibrated ensembles, respectively. To compare two sampled structures  $\mathcal{S}$  and  $\mathcal{S}'$  from each of the ensembles,

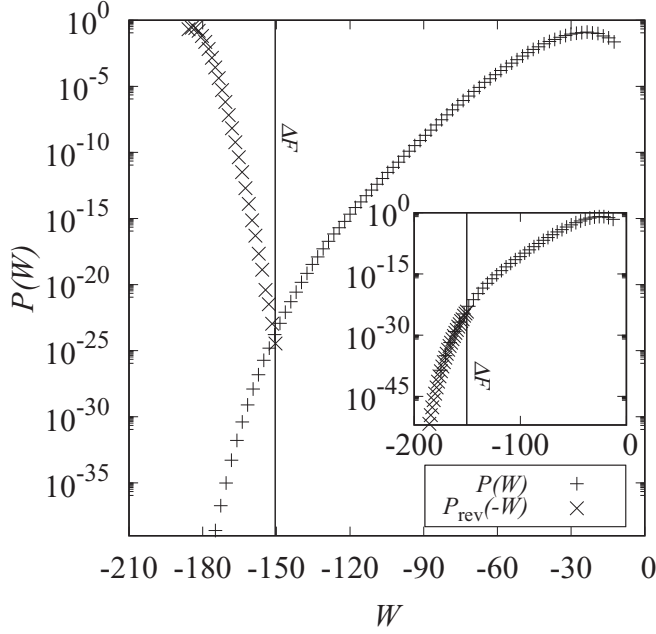


FIG. 4. Plain and mirrored work distributions for  $T = 0.3$  and 16 sweeps of the forward and reverse process, respectively. They intersect near  $W = \Delta F$ , which is the exact value and indicated by the vertical line. The inset shows the same plot but with the distribution for the reverse process (cross symbols) rescaled as  $P_{\text{rev}}(-W) \exp(-(\Delta F - W)/T)$ , according to the Crooks equation, yielding a good agreement with  $P(W)$ .

we define an *overlap*  $\sigma$ , which runs over all bases of the sequence, and counts  $1/L$  if for both structures the base is not paired or if for both structures it is paired with the same base. Otherwise zero is counted. By using the equivalent notations

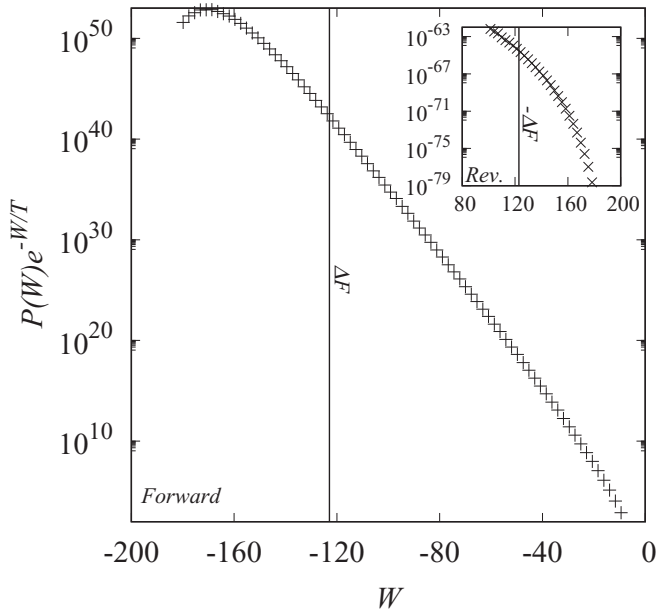


FIG. 5. Jarzynski integrand of the forward process for eight sweeps at  $T = 1$ . Inset: same for the reverse process, in which the maximum is not reached. Error bars are smaller than symbol sizes.

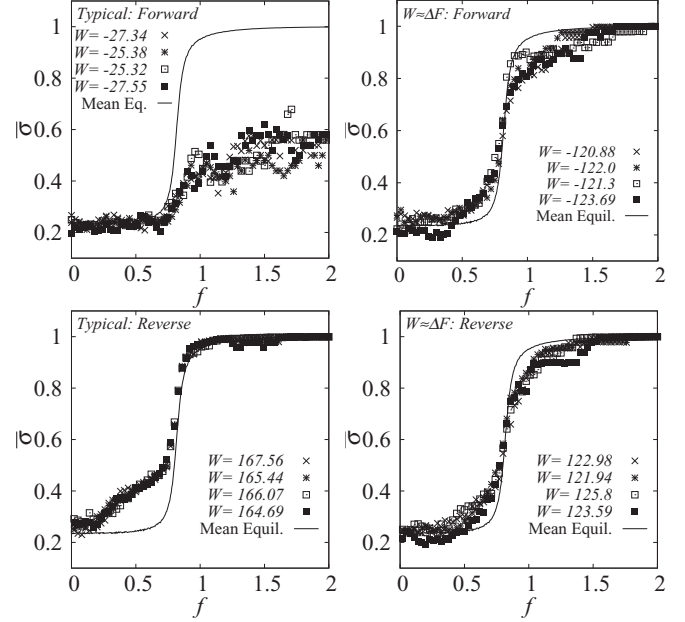


FIG. 6. Average nonequilibrated overlap profiles  $\bar{\sigma}(f)$  for some sample processes at  $T = 1$  and 16 sweeps, with mentioned nonequilibrium work values  $W$ . The average is performed over 100 equilibrium trajectories while keeping the same nonequilibrium one. The solid line is the average overlap between 2500 pairs of independently sampled equilibrium structures for every force value. Top row: forward process for typical values of  $W$  (left) and for  $W \approx \Delta F$  (right). Bottom row: the same for the reverse process. Error bars are smaller than symbol size.

$\{s(i)\}$  and  $\{s'(i)\}$  for the pairing partners of the residues (0 if not paired), the overlap is given by

$$\sigma(\mathcal{S}, \mathcal{S}') = \frac{1}{L} \sum_{i=1}^L \delta_{s(i), s'(i)} \quad (10)$$

where the Kronecker delta is given by  $\delta_{k,l} = 1$  if  $k = l$  and  $\delta_{k,l} = 0$  else. Therefore, two structures are considered as equal for the  $i$ th residue if in both structures the residue is either not paired, or if in both structures it is paired to the same other residue. Note that the other residue of the pair will also contribute positively to the sum, so each pair in the secondary structure actually contributes a value of two. This means the overlap equals one when  $\mathcal{S}, \mathcal{S}'$  denote the same secondary structure, e.g., also for an empty structure. It equals zero when they are completely different. Overlap quantities are used frequently to determine order in complex systems, e.g., spin glass [63].

Figure 6 shows average *nonequilibrium profiles*  $\bar{\sigma}(f)$ , i.e., averaged overlaps  $\sigma$  as function of  $f$ , where in the calculation of the overlaps one structure is a given nonequilibrium sample of a forward or a reverse process and the other structure is a sampled equilibrium structure. The average is always taken over 100 equilibrium structures. The nonequilibrated trajectories are selected by values of  $W$  of interest, i.e., the results are binned by  $W$ . In particular we focus first on *typical* values of  $W$ , i.e., where  $P(W)$  is large, and on  $W \approx \Delta F$ . In the next paragraph we then study the full range of work values. Note that  $\bar{\sigma}(f)$  also reflects the fluctuations of the configurations.



These fluctuations are determined by the ensembles where  $\mathcal{S}$  and  $\mathcal{S}'$  are taken from, respectively. For comparison in all plots the average *equilibrium* profile is shown, where 2500 pairs of independently sampled equilibrium structures were generated for every force value. Our results show that folded structures at low force value  $f$  are characterized by a variety of secondary structures, while at high values of  $f$ , where the RNA is basically stretched, the secondary structures are very similar to each other. Note that for the reverse trajectories in the nonequilibrated case, the overlap is for  $f \rightarrow 0$  slightly higher than the equilibrium value. This is probably due to the fact that the nonequilibrated trajectories contributing the structures  $\mathcal{S}'$  to  $\bar{\sigma}$  are selected with respect to the work  $W$ , i.e., they represent a subensemble with an almost fixed work value. Thus, they overall fluctuate less as compared to the equilibrium structures, where the work fluctuates more. We see that for typical work values (left panels), i.e., where  $P(W)$  and  $P_{\text{rev}}(W)$  peak, large differences for nonequilibrium profiles compared to the average equilibrium profile occur, in particular for the forward process. On the other hand, for work values  $W \approx \Delta F$  (right panels), a much higher similarity is observed. Thus, these nonequilibrium processes, which occur only rarely since  $P(W)$  is very small, exhibit a high similarity to the equilibrium ones.

Note that for work values  $W \approx W_j^*$  also a high similarity is observed. Since these overlap profiles look similar, we do not show them here. Instead we want to quantify the similarity  $I^\sigma$  of the nonequilibrated processes to the equilibrium case for any value of  $W$ . Thus, we integrate over all force values  $f$  the absolute difference of  $\bar{\sigma}(f)$  between the equilibrium and nonequilibrated case, and average this integral over close-by values of  $W$ . Thus, we obtain

$$I^\sigma(W) = \left[ \frac{1}{n_f} \sum_f |\bar{\sigma}(f) - \bar{\sigma}_{Eq}(f)| \right], \quad (11)$$

where the average [...] is over different trajectories exhibiting work values from the same bin  $W$ . The result is shown in Fig. 7, in which rather larger differences for typical values of  $W$  are observed. This is in particular true for the forward process, see also Fig. 6. The reason is that for each sequence of nested pairs only the first-level pair is subject to the force. Thus, when increasing the force, opening pairs below the first level pair it is energetically not favorable. Therefore, basically one pair must be opened after the other, while the remainder of the structure will not change much. Thus, the structure is opened like a zipper, but due to the random update order this takes a while. On the other hand when  $f \rightarrow 0$  is decreased, any formed pair will decouple a certain subsequence from the force, which creates many potential pairs which are energetically favorable. This leads to faster folding, i.e., less MC steps are needed, as compared to unfolding.

Next, near  $W \approx \pm \Delta F$  the similarity is of the order of the similarity  $I_0$  obtained by averaging  $I^\sigma$  over many independent equilibrium processes, which represents the equilibrium fluctuations. Also the forward processes sampled for work values near the value  $W_j^* \approx -170$  where the Jarzynski integrand  $P(W)e^{-W/T}$  peaks exhibit a high similarity to the equilibrium case. Note that for the reverse process, the value of  $W_j^*$  occurs outside our sampled region, thus we do not have processes

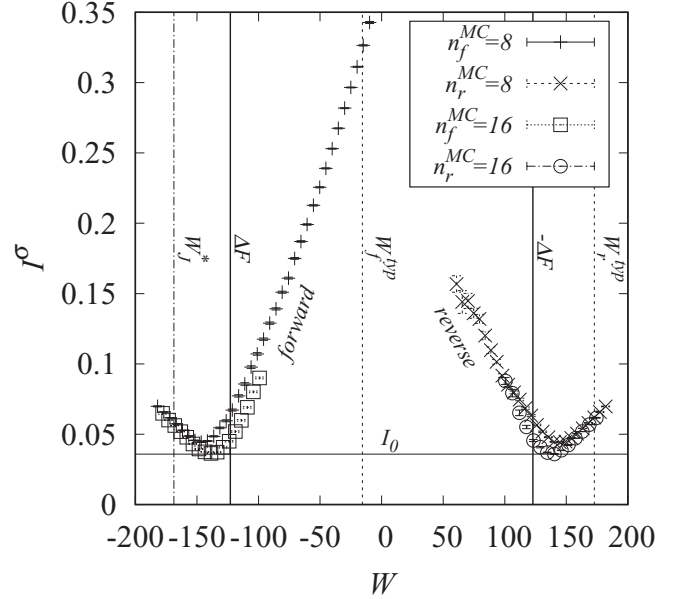


FIG. 7. Integrated difference  $I^\sigma$  between equilibrium and nonequilibrium overlap profiles at  $T = 1$ , for forward (left) and backward (right) processes. For 16 sweeps the data is only partially shown, for better visibility. The horizontal line indicates  $I_0$ , the value of  $I^\sigma$  in equilibrium. Vertical lines indicate work values at (from left to right) the maximum  $W_j^*$  of the Jarzynski integrand, the free energy difference  $\Delta F$ , the maximum  $W_j^{\text{fyp}}$  of the forward process work distribution, the negative free energy difference  $-\Delta F$ , and the maximum point  $W_r^{\text{fyp}}$  of the reverse process work distribution. At eight sweeps there are a total of 90 947 RNA MC runs for the forward and 44 136 for the reverse process. At 16 sweeps there are a total of 50 763 RNA MC runs for the forward and 25 214 for the reverse process.

for this case. For the slower case of  $n_{\text{MC}} = 16$  sweeps, i.e., a bit nearer to equilibrium, the location minimum moves closer to  $\Delta F$  and even decreases in height towards the equilibrium value  $I_0$ .

Thus, our results show that not only do the rare processes near  $W = \pm \Delta F$  have similar work values like the equilibrium processes, they exhibit also very similar sequences, as function of the force  $f$ , of sampled structures. We obtained a similar result when considering force-extension curves.

#### D. Force-extension curves

In addition to the overlap profiles  $\bar{\sigma}(f)$  presented before, we also used force extension curves (FECs)  $n(f)$  to compare processes for equilibrium and nonequilibrated situations. Note that the extension  $n(\mathcal{S})$  of a structure can be very much influenced by single base pairs. Thus two processes, which look very similar on the level of secondary structures, can be very different with respect to force-extension curves.

Samples for equilibrium and nonequilibrated FECs for forward processes, along with corresponding averages, are shown in Fig. 8. For the equilibrium case, a sigmoidal form can be observed, with some fluctuations, and a strong change near the critical force value, where the folding-unfolding transition takes place [29]. For the nonequilibrated case, the

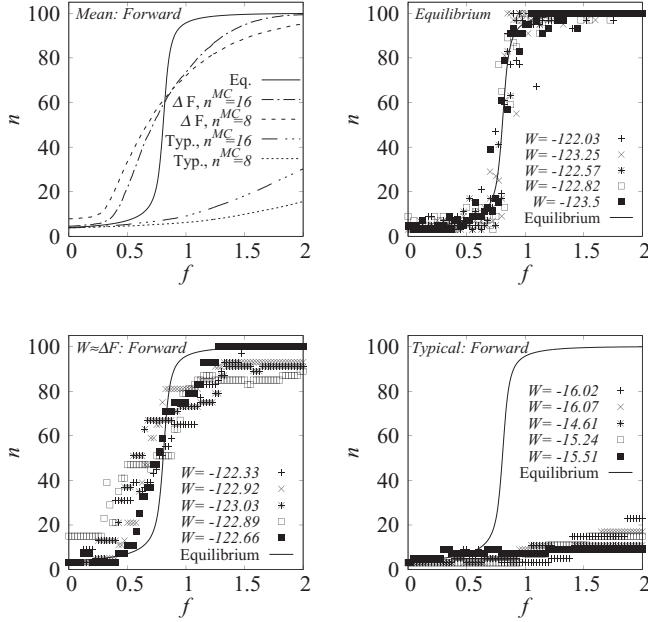


FIG. 8. Top left: mean FECs, in equilibrium as well as in nonequilibrium for typical forward processes and for work values near  $\Delta F$ , for two different numbers  $n_{MC}$  of sweeps at  $T = 1$ . The nonequilibrated FECs that were averaged are selected from a work range  $\pm 1$  around the specified values yielding at least 443 or more contributing RNA MC runs. Top right: samples of such single FECs in equilibrium. Bottom left: samples of nonequilibrated FECs with  $n_{MC} = 8$  for  $W$  near  $\Delta F$ . Bottom right: single, i.e., nonaveraged, samples of typical nonequilibrated FECs, i.e., where  $W \gg \Delta F$ , with  $n_{MC} = 8$ . The solid line represents always the mean equilibrium FEC; see Eq. (5).

typical FECs, i.e., with typical work values  $W$  far from  $\Delta F$ , agree only for small values of  $f$ , i.e., in the initial phase of the process. On the other hand, the rare processes with  $W$  close to  $\Delta F$ , where five different examples are shown here, are much more similar to the equilibrium FECs. Here differences appear mainly near the critical folding-unfolding force.

Samples for equilibrium and nonequilibrated FECs for backward processes, along with corresponding averages, are shown in Fig. 9. The results correspond to the forward case, but the processes with *typical* values of  $W$  agree well with the average equilibrium FEC only for large values of  $f$  but not for small values of  $f$ . This means they also agree in the initial phase of the process, before the critical folding-unfolding force value is reached. The FECs for work values  $W \approx \Delta F$  are also for reverse processes much more similar to the equilibrium case than typical reverse processes.

These results are confirmed by averaging the absolute value of the differences between one FEC  $n(f)$  and the mean equilibrium FEC  $\bar{n}_{Eq}(f)$  over all available values of the force  $f$ , i.e., calculating

$$I^n(W) = \left[ \frac{1}{n_f} \sum_f |n(f) - \bar{n}_{Eq}(f)| \right]. \quad (12)$$

The average [...] is over different realizations of  $n(f)$  exhibiting work values from the same bin  $W$ . Even when considering

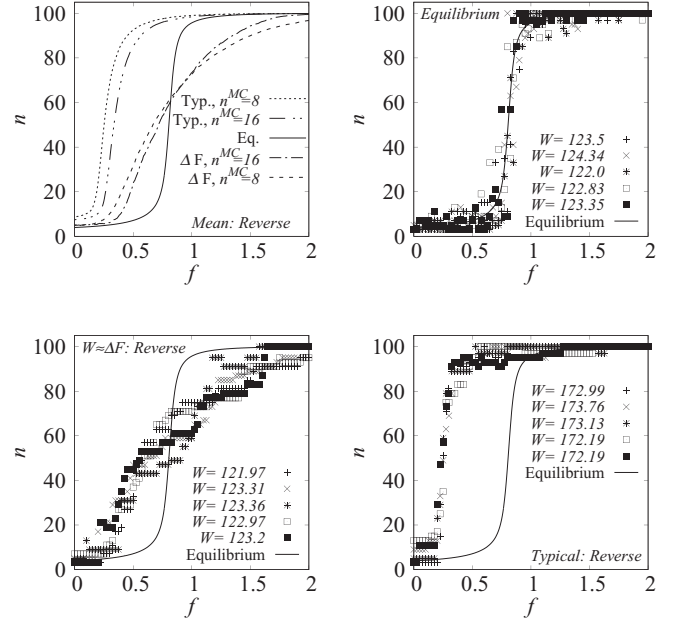


FIG. 9. Top left: mean FECs, in equilibrium as well as in nonequilibrium for typical reverse processes and for work values near  $\Delta F$ , for two different numbers of  $n_{MC}$  of sweeps at  $T = 1$ . The nonequilibrated FECs that were averaged are selected from a work range  $\pm 1$  around the specified values yielding at least 164 or more contributing RNA MC runs. Top right: samples of such single FECs in equilibrium. Bottom left: samples of nonequilibrated reverse FECs with  $n_{MC} = 8$  for  $W$  near  $\Delta F$ . Bottom right: samples of typical non-equilibrated reverse FECs, i.e., where  $W \gg \Delta F$ , with  $n_{MC} = 8$ . The solid line represents always the mean equilibrium FEC as shown already in Fig. 8.

equilibrium FECs for  $n(f)$ , respectively, there is some variation reflected by a nonzero average value  $I_0$ . When using nonequilibrated FECs, with a specified binned value of  $W$ , one sees stronger differences, as visible in Fig. 10. Similar to  $I^\sigma$ , the closest agreements between nonequilibrium and equilibrium are seen near  $W \approx \Delta F$ . In contrast to  $I^\sigma$  the level of the equilibrium fluctuations is not reached for the measurable quantity FEC.

## V. DISCUSSION

RNA unfolding and refolding under influence of an external force for one particular RNA sequence have been studied in exact equilibrium and for nonequilibrated dynamics. The equilibrium trajectories were generated by direct exact sampling, for various values of the external force. The nonequilibrium trajectories were generated by MC dynamics during which the force was changed. For the nonequilibrated case, by using sophisticated large-deviation algorithms, we could access a large range of the support of the probability distribution for the work. This allowed us to confirm the Crooks and Jarzynski theorems over several dozens of decades in probability. Furthermore, we analyzed the trajectories in force-extension as well as in secondary-structure space by selecting according to various values of  $W$ . It was observed that near the most relevant, but very improbable, values of  $W$ , the sampled trajectories reach a high similarity with true

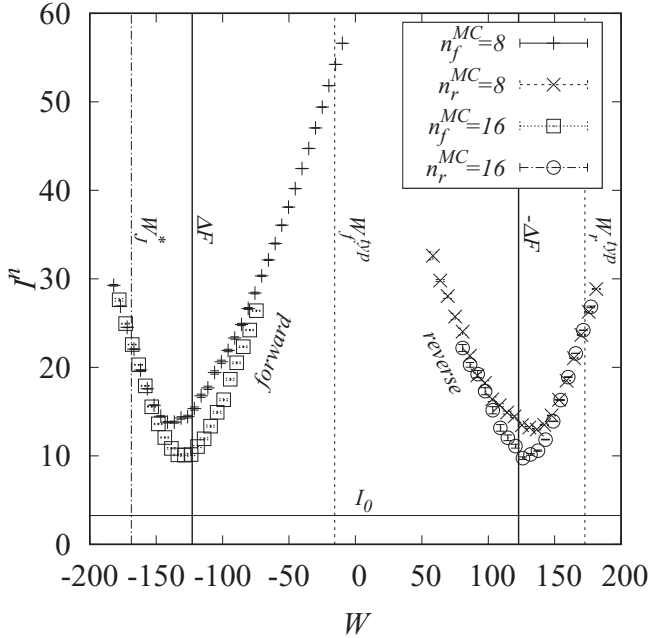


FIG. 10. Integrated extension difference  $I^n$  between averaged equilibrium and nonequilibrium at  $T = 1$ . For eight sweeps the entire work range is plotted, where for 16 sweeps only a range around the minimum is shown, for better visibility.  $I_0$ , represented by a horizontal line, is the averaged value of  $I^n$  when comparing equilibrium FECs to the averaged equilibrium FEC. The left curves represent the forward, the right ones the reverse process. Vertical lines indicate work values at (from left to right) the maximum  $W_J^*$  of the Jarzynski integrand, the free energy difference  $\Delta F$ , the maximum  $W_f^{\text{yp}}$  of the forward process work distribution, the negative free energy difference  $-\Delta F$ , and the maximum point  $W_r^{\text{yp}}$  of the reverse process work distribution. At eight sweeps there are a total of 90 947 RNA MC runs for the forward and 44 136 for the reverse process. At 16 sweeps there are a total of 50 763 RNA MC runs for the forward and 25 214 for the reverse process.

equilibrium. Thus, the study here does not depend on assigning a time-dependent weight to the trajectories as, e.g., in Refs. [24,26,27], the selection is solely by the total work performed during the process and suitably evaluating fluctuation theorems. Also no other particular similarity to equilibrium is enforced explicitly by our procedure. Our approach and results may open a pathway not only to learning about

equilibrium characteristic scalar numbers from nonequilibrium measurements, but also even investigating near-equilibrium dynamics by performing biased nonequilibrium simulations which require only a small number of MC steps. We anticipate that similar studies are feasible and useful for many different types of systems.

Clearly, we have studied so far one particular RNA sequence. Although we expect that in general the closeness of relevant rare-event trajectories to equilibrium carries over, details on the result will certainly depend on the actual sequence. One can imagine that there are biological sequences which fold easily and thus evolve closer to equilibrium anyway. On the other hand, there might be more complex structures, e.g., arising from random sequences, which have an even more complex behavior than the hairpin. Here it would be very interesting to test whether our approach still works and, if so, how close the most relevant trajectories to equilibrium are in this case.

For further studies, also beyond considering RNA secondary structures, one could also extend the approach, by storing the configurations of the close-to-equilibrium  $W \approx \Delta F$  generated rare trajectories. Starting with these configurations, one could perform additional equilibrium simulations at fixed force values, i.e., without performing work, in the hope to get quickly close or even up to equilibrium. We have run some test simulations which show that one can indeed get even much closer to the equilibrium behavior by applying this add-on equilibration, apparently perfectly with respect to the force-extension curves, but this also depends on the temperature. Here more studies are needed, in particular a comparison of how good one can equilibrate by just using secondary-structure RNA MC simulations when starting with empty configurations, i.e., the extended structure without any base pairs. Also it would be very interesting to see how these results depend of the actual RNA sequence and the corresponding energy landscape.

## ACKNOWLEDGMENTS

The simulations were performed at the the HPC cluster CARL, located at the University of Oldenburg (Germany) and funded by the DFG through its Major Research Instrumentation Program (INST 184/157-1 FUGG) and the Ministry of Science and Culture (MWK) of the Lower Saxony State.

[1] J. P. Sethna, *Statistical Mechanics: Entropy, Order Parameters and Complexity* (Oxford University Press, Oxford, 2006).  
 [2] L. Berthier and G. Biroli, *Rev. Mod. Phys.* **83**, 587 (2011).  
 [3] M. Jeng, *Am. J. Phys.* **74**, 514 (2006).  
 [4] C. Jarzynski, *Phys. Rev. Lett.* **78**, 2690 (1997).  
 [5] G. E. Crooks, *J. Stat. Phys.* **90**, 1481 (1998).  
 [6] J. Kurchan, *J. Stat. Mech.* (2007) P07005.  
 [7] U. Seifert, *Eur. Phys. J. B* **64**, 423 (2008).  
 [8] E. M. Sevick, R. Prabhakar, S. R. Williams, and D. J. Searles, *Ann. Rev. Phys. Chem.* **59**, 603 (2008).

[9] C. Jarzynski, *Eur. Phys. J. B* **64**, 331 (2008).  
 [10] M. Esposito, U. Harbola, and S. Mukamel, *Rev. Mod. Phys.* **81**, 1665 (2009).  
 [11] C. Jarzynski, *Annu. Rev. Condens. Matter Phys.* **2**, 329 (2011).  
 [12] U. Seifert, *Rep. Prog. Phys.* **75**, 126001 (2012).  
 [13] R. Marsland III and J. England, *Rep. Prog. Phys.* **81**, 016601 (2018).  
 [14] A. K. Hartmann, *Big Practical Guide to Computer Simulations* (World Scientific, Singapore, 2015).  
 [15] G. Hummer and A. Szabo, *Proc. Natl. Acad. Sci. U. S. A.* **107**, 21441 (2010).

- [16] D. J. Evans, E. G. D. Cohen, and G. P. Morriss, *Phys. Rev. Lett.* **71**, 2401 (1993).
- [17] D. J. Evans and D. J. Searles, *Phys. Rev. E* **50**, 1645 (1994).
- [18] G. Gallavotti and E. G. D. Cohen, *Phys. Rev. Lett.* **74**, 2694 (1995).
- [19] G. Gallavotti and E. G. D. Cohen, *J. Stat. Phys.* **80**, 931 (1995).
- [20] J. Kurchan, *J. Phys. A: Math. Gen.* **31**, 3719 (1998).
- [21] J. L. Lebowitz and H. Spohn, *J. Stat. Phys.* **95**, 333 (1999).
- [22] C. Maes, *J. Stat. Phys.* **95**, 367 (1999).
- [23] G. E. Crooks, *Phys. Rev. E* **60**, 2721 (1999).
- [24] G. E. Crooks, *Phys. Rev. E* **61**, 2361 (2000).
- [25] A. B. Adib, *Phys. Rev. E* **71**, 056128 (2005).
- [26] C. Jarzynski, *Phys. Rev. E* **56**, 5018 (1997).
- [27] G. Hummer and A. Szabo, *Proc. Nat. Acad. Sci. U. S. A.* **98**, 3658 (2001).
- [28] E. Ising, *Z. Phys.* **31**, 253 (1925).
- [29] M. Müller, F. Krzakala, and M. Mézard, *Eur. Phys. J. E* **9**, 67 (2002).
- [30] J. Liphardt, S. Dumont, S. B. Smith, I. Tinoco, and C. Bustamante, *Science* **296**, 1832 (2002).
- [31] D. Collin, F. Ritort, C. Jarzynski, S. B. Smith, I. Tinoco, and C. Bustamante, *Nature (London)* **437**, 231 (2005).
- [32] F. Liu, H. Tong, and Z. Ou-Yang, *Biophys. J.* **90**, 1895 (2006).
- [33] A. K. Hartmann, *Phys. Rev. E* **65**, 056102 (2002).
- [34] J. A. Bucklew, *Introduction to Rare Event Simulation* (Springer-Verlag, New York, 2004).
- [35] C. Dellago, P. G. Bolhuis, F. S. Csajka, and D. Chandler, *J. Chem. Phys.* **108**, 1964 (1998).
- [36] P. G. Bolhuis, D. Chandler, C. Dellago, and P. L. Geissler, *Ann. Rev. Phys. Chem.* **53**, 291 (2002).
- [37] C. Giardinà, J. Kurchan, and L. Peliti, *Phys. Rev. Lett.* **96**, 120603 (2006).
- [38] V. Lecomte and J. Tailleur, *J. Stat. Mech.* (2007) P03004.
- [39] W. Staffeldt and A. K. Hartmann, *Phys. Rev. E* **100**, 062301 (2019).
- [40] A. K. Hartmann, P. L. Doussal, S. N. Majumdar, A. Rosso, and G. Schehr, *Europhys. Lett.* **121**, 67004 (2018).
- [41] A. K. Hartmann, *Phys. Rev. E* **89**, 052103 (2014).
- [42] P. G. Higgs, *Phys. Rev. Lett.* **76**, 704 (1996).
- [43] B. Burghardt and A. K. Hartmann, *Phys. Rev. E* **71**, 021913 (2005).
- [44] R. Lorenz, S. H. Bernhart, C. Höner zu Siederdisen, H. Tafer, C. Flamm, P. F. Stadler, and I. L. Hofacker, *Algor. Mol. Biol.* **6**, 26 (2011).
- [45] I. Tinoco and C. Bustamante, *J. Mol. Biol.* **293**, 271 (1999).
- [46] M. Zuker, *Nucl. Acid Res.* **31**, 3406 (2003).
- [47] Y. Ding, C. Y. Chan, and C. E. Lawrence, *Nucl. Acids Res.* **32**, W135 (2004).
- [48] J. Reuter and D. H. Mathews, *BMC Bioinf.* **11**, 129 (2010).
- [49] U. Gerland, R. Bundschuh, and T. Hwa, *Biophys. J.* **81**, 1324 (2001).
- [50] R. Nussinov, G. Pieczenik, J. R. Griggs, and D. J. Kleitman, *SIAM J. Appl. Math.* **35**, 68 (1978).
- [51] A. P. J. Jansen, *An Introduction to Kinetic Monte Carlo Simulations of Surface Reactions* (Springer, Heidelberg, 2012).
- [52] P. A. Martin, *J. Stat. Phys.* **16**, 149 (1977).
- [53] A. F. Voter, in *Radiation Effects in Solids*, edited by K. E. Sickafus, E. A. Kotomin, and B. P. Uberuaga (Springer, Dordrecht, 2007), pp. 1–23.
- [54] J. A. Mydosh, *Spin Glasses: An Experimental Introduction* (Taylor and Francis, London, 1993).
- [55] M. Faber and S. Klumpp, *Phys. Rev. E* **88**, 052701 (2013).
- [56] G. E. Crooks and D. Chandler, *Phys. Rev. E* **64**, 026109 (2001).
- [57] C. Flamm, W. Fontana, I. L. Hofacker, and P. Schuster, *RNA* **6**, 325 (2000).
- [58] E. E. Dykeman, *Nucl. Acids Res.* **43**, 5708 (2015).
- [59] K. Darty, A. Denise, and Y. Ponty, *Bioinformatics* **25**, 1974 (2009).
- [60] J. Liphardt, B. Onoa, S. B. Smith, I. Tinoco, and C. Bustamante, *Science* **292**, 733 (2001).
- [61] F. Liu and Z. Ou-Yang, *Biophys. J.* **88**, 76 (2005).
- [62] R. Bundschuh and T. Hwa, *Phys. Rev. Lett.* **83**, 1479 (1999).
- [63] M. Mézard, G. Parisi, and M. Virasoro, *Spin Glass Theory and Beyond* (World Scientific, Singapore, 1987).